

Effective (kinetic freeze-out) temperature, transverse flow velocity, and kinetic freeze-out volume in high energy collisions

Muhammad Waqas^{1,2,3,*}, Fu-Hu Liu^{1,2,†}, Li-Li Li^{1,2,‡}, Haidar Mas'ud Alfanda^{4,§}

¹*Institute of Theoretical Physics & State Key Laboratory of Quantum Optics and Quantum Optics Devices, Shanxi University, Taiyuan, Shanxi 030006, People's Republic of China*

²*Collaborative Innovation Center of Extreme Optics, Shanxi University, Taiyuan, Shanxi 030006, People's Republic of China*

³*School of Nuclear Science and Technology, University of Chinese Academy of Sciences, Beijing 100049, People's Republic of China*

⁴*Key Laboratory of Quark and Lepton Physics (MOE) & Institute of Particle Physics, Central China Normal University, Wuhan, Hubei 430079, People's Republic of China*

Abstract: The transverse momentum spectra of different types of particles produced in central and peripheral gold-gold (Au-Au) and inelastic proton-proton (pp) collisions at the Relativistic Heavy Ion Collider (RHIC), as well as in central and peripheral lead-lead (Pb-Pb) and pp collisions at the Large Hadron Collider (LHC) are analyzed by the multi-component standard (Boltzmann-Gibbs, Fermi-Dirac, and Bose-Einstein) distribution. The obtained results from the standard distribution give an approximate agreement with the measured experimental data by the STAR, PHENIX, and ALICE Collaborations. The behavior of the effective (kinetic freeze-out) temperature, transverse flow velocity, and kinetic freeze-out volume with the mass for different particles is obtained, which observes the early kinetic freeze-out of heavier particles as compared to the lighter particles. The parameters of emissions of different particles are observed to be different, which reveals a direct signature of the mass dependent differential kinetic freeze-out. It is also observed that the peripheral nucleus-nucleus (AA) and pp collisions at the same center-of-mass energy per nucleon pair are close in terms of the extracted parameters.

Keywords: Transverse momentum spectra, effective temperature, kinetic freeze-out temperature, transverse flow velocity, kinetic freeze-out volume

PACS: 12.40.Ee, 14.40.Aq, 24.10.Pa, 25.75.Ag

1 Introduction

A hot and dense fireball is assumed to form for a brief period of time (\sim a few fm/ c) over an extended region after the initial collisions, which undergoes a collective expansion which leads to the change in the temperature and volume or density of the system. Three types of temperatures namely the initial temperature, chemical freeze-out temperature, and kinetic freeze-out temperature can be found in the literature, which describe the excitation degrees of interacting system at the stages of initial collisions, chemical freeze-out, and kinetic freeze-

out respectively [1, 2, 3, 4, 5, 6, 7]. There is another type of temperature, named the effective temperature, which is not a real temperature and it describes the sum of excitation degree of the interacting system and the effect of transverse flow at the stage of kinetic freeze-out.

In principle, the initial stage of collisions happens earlier than other stages such as the chemical and kinetic freeze-out stages. Naturally, the initial temperature is the largest and the kinetic freeze-out temperature is the lowest among the three real temperatures, while the chemical freeze-out temperature is in between the initial and kinetic freeze-out temperatures. It does

*E-mail: waqas_phy313@yahoo.com

†Corresponding author. E-mail: fuhuliu@163.com; fuhuliu@sxu.edu.cn

‡E-mail: shanxi-lll@qq.com

§E-mail: hmasud@mails.ccnu.edu.cn

not get rid of the simultaneity for chemical and kinetic freeze-outs, which results in the chemical and kinetic freeze-out temperatures to be the same. The effective temperature is often larger than the kinetic freeze-out temperature but it is equal to kinetic freeze-out temperature in case of zero transverse flow velocity.

To conceive the given nature of the nuclear force and to break the system into massive fragments [8, 9], it is a good way to bring the nucleons in interactions in nucleus-nucleus (AA) collisions at intermediate and high energies and such a process provokes a liquid-gas type phase transition because lots of nucleons and other light nuclei are emitted. In AA collisions at higher energies, a phase transition from hadronic matter to quark-gluon plasma (QGP) is expected to occur. The volume occupied by such ejectiles source where the mutual nuclear interactions become negligible (they only feel the coulombic repulsive force and are free from the attractive force) is said to be kinetic freeze-out volume and it has been introduced in various statistical and thermodynamic models [10, 11]. Like the kinetic freeze-out temperature, the kinetic freeze-out volume also gives the information of the co-existence of phase transition. This is one of the major quantities, which is important in the extraction of vital observables such as multiplicity, micro canonical heat capacity, and its negative branch or shape of caloric curves under the external constraints [12, 13, 14, 15, 16].

It is conceivable that the temperature (volume) of the interacting system decreases (increases) from the initial state to the latest kinetic freeze-out stage. During the evolution process, the transverse flow velocity is existent due to the expansion of the interacting system. The study of dependence of effective (kinetic freeze-out) temperature, transverse flow velocity, and kinetic freeze-out volume on collision energy, event centrality, system size, and particle rapidity is very significant. We are very interested in the mentioned quantities in central and peripheral AA and (inelastic) proton-proton (pp) collisions at the Relativistic Heavy Ion Collider (RHIC) and the Large Hadron Collider (LHC) over a wide enough energy range in which QGP is expected to form.

In this paper, we study the dependence of effective (kinetic freeze-out) temperature, transverse flow velocity, and kinetic freeze-out volume in central and peripheral gold-gold (Au-Au) and lead-lead (Pb-Pb) collisions at the RHIC and LHC energies and compare their peripheral collisions with pp collisions of the same center-

of-mass energy per nucleon pair $\sqrt{s_{NN}}$ (or the center-of-mass energy \sqrt{s} for pp collisions). Only 62.4 GeV at the RHIC and 5.02 TeV at the LHC are considered as examples. We present the approach of effective temperature and kinetic freeze-out volume from the transverse momentum spectra of the identified particles produced in the mentioned AA and pp collisions. The kinetic freeze-out temperature and transverse flow velocity are then obtained from particular linear relations.

The remainder of this paper is structured as follows. The formalism and method are described in Section 2. Results and discussion are given in Section 3. In Section 4, we summarize our main observations and conclusions.

2 The method and formalism

Generally, two main processes of particle production are under consideration, which includes the soft and hard excitation processes. The soft excitation process is the strong interactions among multiple partons, while the hard excitation process is the more violent collisions between two head-on partons. The soft excitation process has numerous choices of formalisms, including but are not limited to the Hagedorn thermal model (Statistical-bootstrap model) [17], the (multi-)standard distribution [18], the Tsallis and related distributions with various formalisms [19], the blast-wave model with Tsallis statistics [20], the blast-wave model with Boltzmann statistics [21, 22, 23, 26, 29], and other thermodynamic related models [30, 31, 32, 33]. The hard excitation process has very limited choice of formalisms and can be described by the perturbative quantum chromodynamics (pQCD) [34, 35, 36].

The experimental data of the transverse momentum (p_T) spectrum of the particles are fitted by using the standard distribution which is the joint name of Boltzmann-Gibbs, Fermi-Dirac, and Bose-Einstein distributions which correspond to the factor $S = 0, +1$, and -1 , respectively. The standard distribution at the mid-rapidity can be demonstrated as [18]

$$f_S(p_T) = \frac{1}{N} \frac{dN}{dp_T} = \frac{1}{N} \frac{gV'}{(2\pi)^2 p_T} \sqrt{p_T^2 + m_0^2} \times \left[\exp \left(\frac{\sqrt{p_T^2 + m_0^2}}{T} \right) + S \right]^{-1} \quad (1)$$

in which the chemical potential is neglected, where N is the experimental number of considered particles, T is the fitted effective temperature, V' is the fitted kinetic freeze-out volume (i.e. the interaction volume) of

the emission source at the stage of kinetic freeze-out, $g = 3$ (or 2) is the degeneracy factor for pion and kaon (or proton), and m_0 is the rest mass of the considered particle. As a probability density function, the integral of Eq. (1) is naturally normalized to 1, i.e., we have $\int_0^{p_{T\max}} f_S(p_T) dp_T = 1$, where $p_{T\max}$ denotes the maximum p_T . At very high energy, the influence of $S = +1$ and -1 can be neglected. Only the Boltzmann-Gibbs distribution is sufficient to describe the spectra at the RHIC and LHC.

Considering the experimental rapidity range $[y_{\min}, y_{\max}]$ around the mid-rapidity, we have the accurate form of Eq. (1) to be

$$f_S(p_T) = \frac{1}{N} \frac{gV'}{(2\pi)^2} p_T \int_{y_{\min}}^{y_{\max}} \left(\sqrt{p_T^2 + m_0^2} \cosh y - \mu \right) \times \left[\exp \left(\frac{\sqrt{p_T^2 + m_0^2} \cosh y - \mu}{T} \right) + S \right]^{-1} dy, \quad (2)$$

where the chemical potential μ is particle dependent, which was studied by us recently [37]. In high energy collisions, μ_j ($j = \pi, K$, and p) are less than several MeV, which affects slightly V' comparing with that for $\mu_j = 0$. Then, we may regard $\mu \approx 0$ in Eq. (2) at high energies considered in the present work. In Eqs. (1) and (2), only T and V' are free parameters.

Usually, we have to use the two-component standard distribution because single component standard distribution is not enough for the simultaneous description of very low- ($0 \sim 0.2 - 0.3$ GeV/ c) and low- p_T ($0.2 - 0.3 \sim 2 - 3$ GeV/ c or little more) regions, which are contributed by the resonance decays and other soft excitation processes respectively. More than two or multi-component standard distribution can also be used in some cases. We have the simplified multi-component (l -component) standard distribution to be

$$f_S(p_T) = \sum_{i=1}^l k_i \frac{1}{N_i} \frac{gV'_i}{(2\pi)^2} p_T \sqrt{p_T^2 + m_0^2} \times \left[\exp \left(\frac{\sqrt{p_T^2 + m_0^2}}{T_i} \right) + S \right]^{-1}, \quad (3)$$

where N_i and k_i denote respectively the particle number and fraction contributed by the i -th component, and T_i and V'_i denote respectively the effective temperature and kinetic freeze-out volume corresponding to the i -th component.

More accurate form of l -component standard distribution

can be written as,

$$f_S(p_T) = \sum_{i=1}^l k_i \frac{1}{N_i} \frac{gV'_i}{(2\pi)^2} p_T \times \int_{y_{\min}}^{y_{\max}} \left(\sqrt{p_T^2 + m_0^2} \cosh y - \mu \right) \times \left[\exp \left(\frac{\sqrt{p_T^2 + m_0^2} \cosh y - \mu}{T_i} \right) + S \right]^{-1} dy. \quad (4)$$

In Eqs. (3) and (4), only T_i , V'_i and k_i ($i \leq l - 1$) are free parameters. Generally, $l = 2$ or 3 is enough for describing the spectra in a not too wide p_T range.

In fact, Eqs. (1) or (2) and (3) or (4) can be used for the description of p_T spectra and for the extraction of effective temperature and kinetic freeze-out volume in very low- and low- p_T regions. The high- p_T ($> 3 - 4$ GeV/ c) region contributed by the hard excitation process has to be fitted by the Hagedorn function [17] which is an inverse power law

$$f_H(p_T) = \frac{1}{N} \frac{dN}{dp_T} = A p_T \left(1 + \frac{p_T}{p_0} \right)^{-n} \quad (5)$$

which is resulted from the pQCD [34, 35, 36], where A is the normalization constant, which depends on the free parameters p_0 and n , and it results in $\int_0^{p_{T\max}} f_H(p_T) dp_T = 1$.

In case of considering the contributions of both the soft and hard excitation processes, we use the superposition in principle

$$f_0(p_T) = k f_S(p_T) + (1 - k) f_H(p_T), \quad (6)$$

where k is the contribution ratio of the soft process and gives a natural result in $\int_0^{p_{T\max}} f_0(p_T) dp_T = 1$. In Eq. (6), the contribution of soft process is from 0 to $\sim 2 - 3$ GeV/ c , or even to $\sim 3 - 5$ GeV/ c at very high energy, and the hard component contributes the whole p_T range. There are some mixtures between the contributions of the two processes in low- p_T region.

According to the Hagedorn model [17], the contributions of the two processes can be separated completely. One has another superposition

$$f_0(p_T) = A_1 \theta(p_1 - p_T) f_S(p_T) + A_2 \theta(p_T - p_1) f_H(p_T), \quad (7)$$

where $\theta(x)$ is the usual step function, and A_1 and A_2 are the normalization constants which make $A_1 f_S(p_1) = A_2 f_H(p_1)$. Equation (7) gives the contribution of soft process from 0 to p_1 , while the hard component contributes from p_1 up to the maximum.

In the above two two-component functions (Eqs. (6) and (7)), each component ($f_S(p_T)$ and $f_H(p_T)$) is a traditional distribution. In fact, the first component ($f_S(p_T)$) is one of the Boltzmann-Gibbs, Fermi-Dirac, and Bose-Einstein distributions if we use a given S such as $S = 0, +1$, and -1 . The second component ($f_H(p_T)$) is the Tsallis-like distribution [19] if we let $n = 1/(q-1)$ and $p_0 = nT_T$, where q is the entropy index and T_T is the Tsallis temperature.

We will use only the first component in Eq. (7) due to the reason, we do not study a very wide p_T range in the present work. In the case of neglecting the contribution of hard component in low- p_T region in Eq. (6), the first component in Eq. (6) gives the same result as the first component in Eq. (7). In fact, Eq. (4) with $l = 2$, that is the two-component standard distribution, is used in the present work. In addition, considering the treatment of normalization, the real fitted kinetic freeze-out volume should be $V_1 = N_1 V_1'/k_1$ and $V_2 = N_2 V_2'/(1-k_1)$ which will be simply used in the following section.

It should be noted that the value of l in the l -component standard distribution has some influences on the free parameters and then the derived parameters. Generally, $l = 1$ is not enough to fit the particle spectra. In the case of using $l = 2$, the influence of the second component is obvious due to the fact that the contribution of the first component is not enough to fit the particle spectra. In the case of using $l = 3$, the influence of the third component is slight due to the fact that the main contribution is from the first two components, and the contribution of the third component can be neglected.

3 Results and discussion

3.1 Comparison with the data

Figures 1(a) and 1(b) demonstrate the transverse momentum spectra, $(1/2\pi p_T)d^2N/dp_T dy$, of the negatively charged particles π^- , K^- , and \bar{p} produced in (a) central (0–10%) and (b) peripheral (40–80%) Au-Au collisions at $\sqrt{s_{NN}} = 62.4$ GeV. The circles, triangles, and squares represent the experimental data measured in the mid-rapidity range $-0.5 < y < 0$ at the RHIC by the STAR Collaboration [38]. The curves are our fitted results by Eq. (4) with $l = 2$. Following each panel, the results of Data/Fit are presented. The values of the related parameters (T_1 , T_2 , V_1 , V_2 , k_1 , and N_0) along

with the χ^2 and number of degree of freedom (ndof) are given in Table 1. It can be seen that the two-component standard distribution fits approximately the experimental data measured at mid-rapidity in Au-Au collisions at the RHIC.

To see the contributions of the two components in Eq. (4) with $l = 2$, as examples, Figs. 1(c) and 1(d) show the contributions of the first and second components by the dashed and dotted curves respectively, and the total contribution is given by the solid curves. Only the results of π^- produced in (c) central (0–10%) and (d) peripheral (40–80%) Au-Au collisions at $\sqrt{s_{NN}} = 62.4$ GeV are presented. The circles represented the same data points as Figs. 1(a) and 1(b). One can see that the first component contributes mainly in the very low- and low- p_T region, while the second component contributes in a wider region. There are large overlap region of the two contributions.

The transverse momentum spectra, $(1/N_{ev})d^2N/dp_T dy$, of π^- , K^- , and \bar{p} produced in (a) central (0–5%) and (b) peripheral (80–90%) Pb-Pb collisions at $\sqrt{s_{NN}} = 5.02$ TeV are shown in Figure 2, where N_{ev} on the vertical axis denotes the number of events. The experimental data of π^- , K^- , and \bar{p} measured in the mid-rapidity range $|y| < 0.5$ at the LHC by the ALICE Collaboration [39, 40] are represented by the circles, triangles, and squares, respectively. The curves are our results fitted by Eq. (4) with $l = 2$. Following each panel, the results of Data/Fit are presented. The values of the related parameters along with the χ^2 and ndof are given in Table 1. One can see that the two-component standard distribution fits approximately the experimental data measured at mid-rapidity in Pb-Pb collisions at the LHC.

It seems that Figures 1 and 2 for peripheral collisions show the worse fits compared to central collisions. This is caused by a statistical fluctuation and the effect of cold spectator in peripheral collisions. In the region of cold spectator, particles are produced by the multiple cascade scattering process which is different from the thermalization process of particle production in the region of hot participant. In addition, our fits are done in all ranges of $p_T < 4.5$ GeV/ c . However, as an alternative model, the blast-wave fit takes different cuts of p_T for the analysis of different particles (see for instance ref. [2]). These different cuts affect the extractions of parameters, in particular for the analysis of the trends of particles, which is not our expectation.

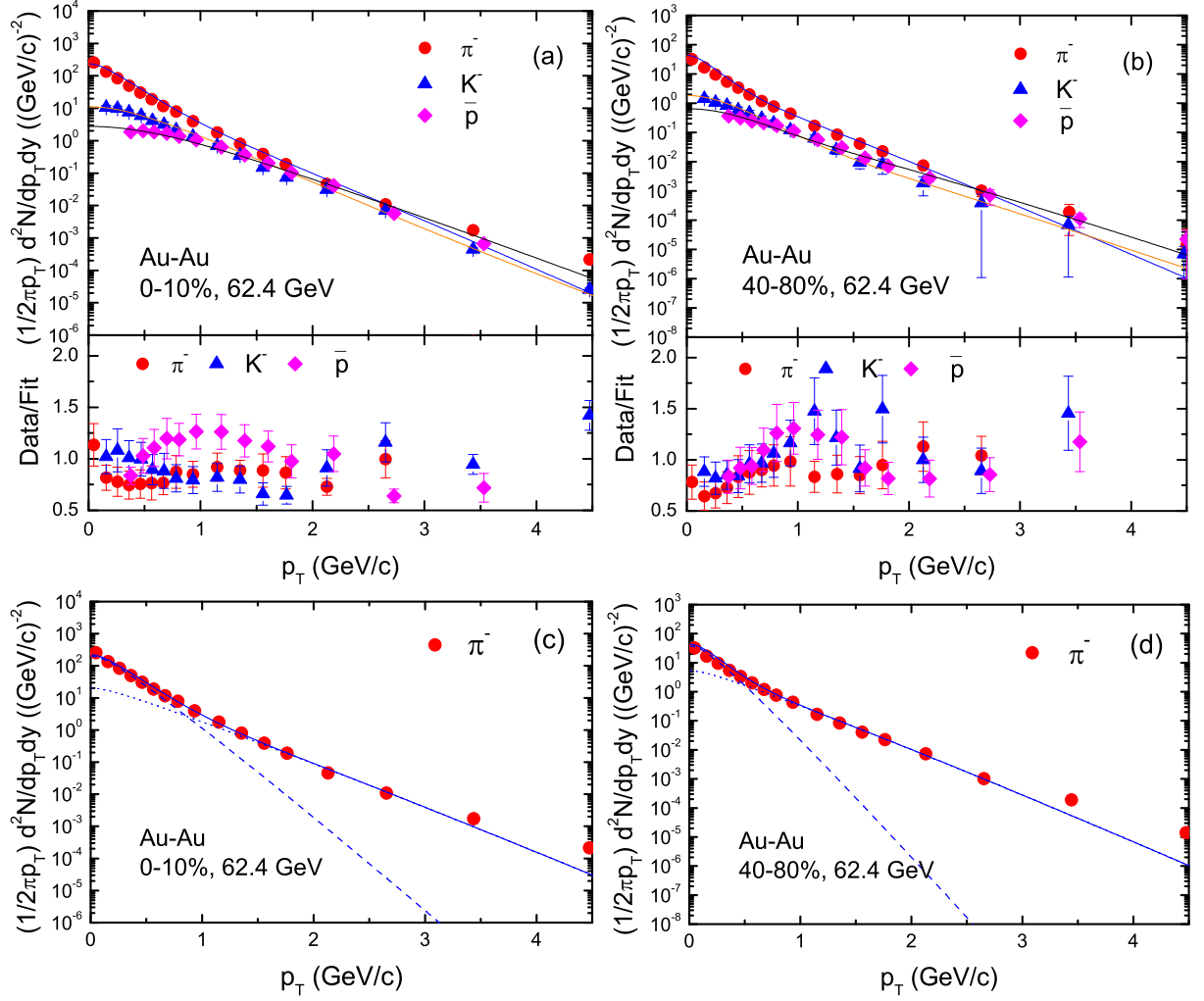


Fig. 1. (a)(b) Transverse momentum spectra of π^- , K^- , and \bar{p} produced in (a) central (0–10%) and (b) peripheral (40–80%) Au-Au collisions at $\sqrt{s_{NN}} = 62.4$ GeV. The symbols represent the experimental data measured in $-0.5 < y < 0$ at the RHIC by the STAR Collaboration [38]. The curves are our fitted results by Eq. (4) with $l = 2$. Following each panel, the results of Data/Fit are presented. (c)(d) As examples, panels (c) and (d) show the contributions of the first and second components in Eq. (4) with $l = 2$ by the dashed and dotted curves respectively, and the total contribution is given by the solid curves. The circles in panels (c) and (d) redisplay those in panels (a) and (b) respectively.

In the next fits, we also use all ranges of $p_T < 4.5$ GeV/c. Figures 3(a) and 3(b) show the transverse momentum spectra, $E d^3\sigma/dp^3 = (1/2\pi p_T) d^2\sigma/dp_T dy$, of π^- , K^- , and \bar{p} produced in pp collisions at $\sqrt{s} = 62.4$ GeV and 5.02 TeV respectively, where E and σ on the vertical axis denote the energy and cross-section respectively. The symbols represent the experimental data measured in the mid-pseudorapidity range $|\eta| < 0.35$ by the PHENIX Collaboration [41] and in the mid-rapidity range $|y| < 0.5$ by the ALICE Collaborations [39, 40]. The curves are our results fitted by Eq. (4) with $l = 2$. Following each panel, the results of Data/Fit are pre-

sented. The values of the related parameters (N_0 in Figs. 1 and 2 is replaced by σ_0 in Fig. 3) along with the χ^2 and ndof are given in Table 1. One can see that the two-component standard distribution fits approximately the experimental data measured at mid-(pseudo)rapidity in pp collisions at the RHIC and LHC.

We would like to point out that the vertical axes of Figs. 1–3 are not the probability density function. We cannot fit them with Eq. (4) with $l = 2$ directly. In fact, we have done a conversion during our fitting. For Fig. 1, we have used the relation $(1/2\pi p_T)(d^2N/dp_T dy) = (1/2\pi p_T)N_0 f_S(p_T)/dy$ in the

Table 1. Values of parameters (T_1 , T_2 , V_1 , V_2 , k_1 , and N_0 (for Figs. 1 and 2) or σ_0 (for Fig. 3)), χ^2 , and ndof corresponding to the solid curves in Figs. 1–3. From the table, we have $k_2 = 1 - k_1$, $T = k_1 T_1 + k_2 T_2$, and $V = V_1 + V_2$. The normalization constants contributed by the first and second components are $k_1 N_0$ (or $k_1 \sigma_0$) and $k_2 N_0$ (or $k_2 \sigma_0$) respectively.

Collisions	Centrality	Particle	T_1 (GeV)	T_2 (GeV)	V_1 (fm ³)	V_2 (fm ³)	k_1	N_0 [σ_0 (mb)]	χ^2	ndof
Figure 1 Au-Au 62.4 GeV	0–10%	π^-	0.141 ± 0.008	0.285 ± 0.007	185 ± 13	3330 ± 270	0.88 ± 0.07	0.080 ± 0.004	43	14
		K^-	0.199 ± 0.009	0.316 ± 0.007	19 ± 1	2034 ± 162	0.85 ± 0.11	0.010 ± 0.003	174	13
		\bar{p}	0.280 ± 0.012	0.340 ± 0.004	22 ± 3	1053 ± 100	0.92 ± 0.10	0.020 ± 0.004	56	11
	40–80%	π^-	0.070 ± 0.006	0.250 ± 0.006	32 ± 5	127 ± 14	0.70 ± 0.07	0.025 ± 0.050	94	14
		K^-	0.239 ± 0.008	0.260 ± 0.004	2.3 ± 0.3	118 ± 18	0.89 ± 0.09	0.005 ± 0.001	40	13
		\bar{p}	0.201 ± 0.007	0.302 ± 0.005	3.0 ± 0.2	69 ± 8	0.89 ± 0.11	0.009 ± 0.001	7	11
Figure 2 Pb-Pb 5.02 TeV	0–5%	π^-	0.267 ± 0.013	0.624 ± 0.005	8943 ± 655	4341 ± 200	0.93 ± 0.12	1.770 ± 0.300	425	33
		K^-	0.355 ± 0.014	0.465 ± 0.006	1820 ± 250	5555 ± 300	0.94 ± 0.12	0.300 ± 0.040	776	32
		\bar{p}	0.459 ± 0.014	0.512 ± 0.006	381 ± 30	5476 ± 240	0.94 ± 0.10	0.325 ± 0.040	748	30
	80–90%	π^-	0.200 ± 0.009	0.407 ± 0.004	154 ± 8	246 ± 50	0.70 ± 0.09	0.060 ± 0.003	658	33
		K^-	0.198 ± 0.016	0.420 ± 0.005	17 ± 2	264 ± 45	0.90 ± 0.11	0.020 ± 0.003	90	32
		\bar{p}	0.302 ± 0.018	0.400 ± 0.006	4.4 ± 0.5	330 ± 56	0.92 ± 0.13	0.008 ± 0.001	296	29
Figure 3(a) pp 62.4 GeV	—	π^-	0.182 ± 0.006	0.275 ± 0.005	65 ± 8	22 ± 4	0.68 ± 0.12	0.350 ± 0.060	54	23
		K^-	0.160 ± 0.007	0.255 ± 0.006	5.0 ± 0.4	77 ± 10	0.88 ± 0.15	0.007 ± 0.001	4	13
		\bar{p}	0.235 ± 0.008	0.260 ± 0.006	1.6 ± 0.1	50 ± 6	0.95 ± 0.10	0.008 ± 0.001	126	24
Figure 3(b) pp 5.02 TeV	—	π^-	0.090 ± 0.008	0.370 ± 0.005	16 ± 2	101 ± 13	0.64 ± 0.11	0.016 ± 0.003	945	33
		K^-	0.850 ± 0.013	0.370 ± 0.004	0.80 ± 0.04	97 ± 12	0.87 ± 0.11	0.007 ± 0.001	666	31
		\bar{p}	0.539 ± 0.010	0.391 ± 0.005	1.1 ± 0.1	77 ± 12	0.90 ± 0.13	0.003 ± 0.001	496	29

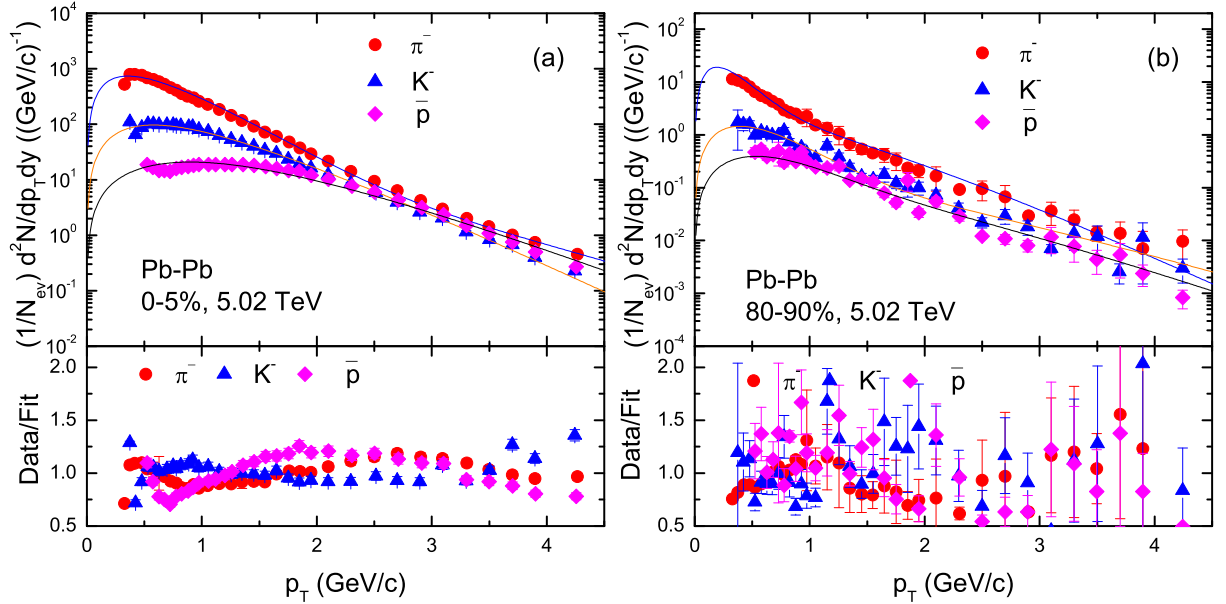


Fig. 2. Transverse momentum spectra of π^- , K^- , and \bar{p} produced in (a) central (0–5%) and (b) peripheral (80–90%) Pb-Pb collisions at $\sqrt{s_{NN}} = 5.02$ TeV. The symbols represent the experimental data measured in $|y| < 0.5$ at the LHC by the ALICE Collaboration [39, 40]. The curves are our results fitted by Eq. (4) with $l = 2$. Following each panel, the results of Data/Fit are presented.

conversion, where N_0 is the normalization constant in terms of particle number. For Fig. 2, we have used the relation $d^2N/dp_T dy = N_0 f_S(p_T)/dy$ in the conversion, where N_{ev} on the vertical axis is neglected because $d^2N/dp_T dy$ is directly regarded as the result per event. For Fig. 3, we have used the relation $Ed^3\sigma/dp^3 = (1/2\pi p_T)(d^2\sigma/dp_T dy) = (1/2\pi p_T)\sigma_0 f_S(p_T)/dy$ in the conversion, where σ_0 is the normalization constant in

terms of cross section.

From Figures 1–3 and Table 1 one can see that the fit qualities in some cases are not very well. It should be point out that the model used in the fits is for soft processes but analyze p_T spectra up to 4.5 GeV/c. The highest values of p_T analyzed contain hard processes which could produce bad fit as indicated by χ^2 in Table 1 and also in the ratio data to fit of Figs. 1–3, then

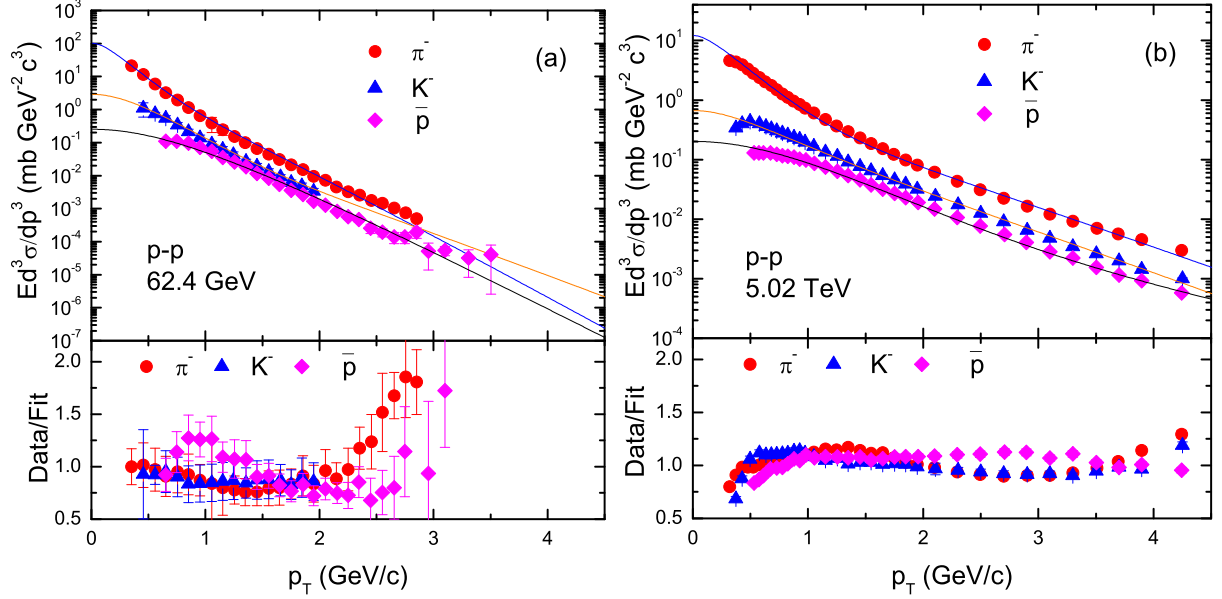


Fig. 3. Transverse momentum spectra of π^- , K^- , and \bar{p} produced in pp collisions at (a) $\sqrt{s} = 62.4$ GeV and (b) $\sqrt{s} = 5.02$ TeV. The symbols represent the experimental data measured in $|\eta| < 0.35$ by the PHENIX Collaboration [41] and in $|y| < 0.5$ by the ALICE Collaborations [39, 40]. The curves are our results fitted by Eq. (4) with $l = 2$. Following each panel, the results of Data/Fit are presented.

maybe seems necessary to fit taking into account the function part corresponding to the hard process. In fact, the hard process is not necessary for extracting the parameters of soft process. Although the fits will be better if we also consider the contribution of hard process, it is not useful for extracting the parameters considered in the present work. Therefore, we give up to study the contribution of hard process.

3.2 Discussion on the parameters

Considering the contributions of the two components, the effective temperature averaged over the two components is $T = k_1 T_1 + k_2 T_2$ and the kinetic freeze-out volume by adding the two components is $V = V_1 + V_2$. Further, the normalization constants contributed by the first and second components are $k_1 N_0$ and $k_2 N_0$ respectively.

For convenience sake, we introduce the average p_T ($\langle p_T \rangle$) and average moving mass (\overline{m} , i.e. average energy in the source rest frame) here. Considering Eq. (4) only, we have

$$\langle p_T \rangle = \int_0^{p_T^{\max}} p_T f_S(p_T) dp_T. \quad (8)$$

To obtain \overline{m} , we may use the Monte Carlo method. Let R_1 and R_2 denote random numbers distributed evenly

in $[0,1]$. A concrete value of p_T which satisfies Eq. (4) can be obtained by

$$\int_0^{p_T} f_S(p'_T) dp'_T < R_1 < \int_0^{p_T + \delta p_T} f_S(p'_T) dp'_T, \quad (9)$$

where δp_T denotes a small shift relative to p_T . In the source rest frame and under the assumption of isotropic emission, the emission angle θ of the considered particle obeys

$$f_\theta(\theta) = \frac{1}{2} \sin \theta \quad (10)$$

which results in

$$\theta = 2 \arcsin(\sqrt{R_2}) \quad (11)$$

in the Monte Carlo method [42]. Then,

$$m = \sqrt{(p_T / \sin \theta)^2 + m_0^2}. \quad (12)$$

After repetition calculation by many times, we may obtain \overline{m} .

To study the change trends of parameters with the particle mass, Figures 4(a) and 4(b) show the dependences of T on m_0 for productions of negative charged particles in central and peripheral (a) Au-Au collisions at 62.4 GeV and (b) Pb-Pb collisions at 5.02 TeV, while pp collisions at (a) 62.4 GeV and (b) 5.02 TeV are also studied and compared to peripheral AA collisions of the

same energy (per nucleon pair). Correspondingly, Figures 4(c) and 4(d) show the dependences of $\langle p_T \rangle$ on \bar{m} for the mentioned particles in the considered collisions. The filled, empty, and half filled symbols represent central and peripheral AA and pp collisions respectively. The lines are our linear fittings on the relations. The related linear fitting parameters are listed in Table 2, though some of them are not good fitting due to very large χ^2 . The intercept in the linear relation between T and m_0 is regarded as the kinetic freeze-out temperature T_0 , and the slope in the linear relation between $\langle p_T \rangle$ and \bar{m} is regarded as the transverse flow velocity β_T . That is $T = am_0 + T_0$ [26, 27, 28] and $\langle p_T \rangle = \beta_T \bar{m} + b$, where a and b are free parameters.

It should be noted that the relation $T = am_0 + T_0$ [26, 27, 28] is used because the intercept should be the kinetic freeze-out temperature T_0 which corresponds to the emission of massless particles for which there is no influence of flow effect. The relation $\langle p_T \rangle = \beta_T \bar{m} + b$ is used by us in our previous works [22, 23, 24, 25] according to the same dimension of $\langle p_T \rangle$ and $\beta_T \bar{m}$. The meanings of the slope a in $T = am_0 + T_0$ and the intercept b in $\langle p_T \rangle = \beta_T \bar{m} + b$ are not clear for us. Maybe, am_0 reflects the effective temperature contributed by flow effect, and b reflects the average transverse momentum contributed by the thermal motion.

From Figure 4 and Table 2 one can see that T (T_0 or β_T) is larger in central AA collisions as compared to peripheral AA collisions, and peripheral AA collisions are comparable with the pp collisions at the same $\sqrt{s_{NN}}$ (\sqrt{s}). The mass dependent or differential kinetic freeze-out scenario on T is observed, as T increases with the increase of m_0 . The present work conforms various mass dependent or differential kinetic freeze-out scenarios [2, 3, 20, 43, 44]. Because T_0 (β_T) is obtained from the linear relation between T and m_0 ($\langle p_T \rangle$ and \bar{m}), it seems that there is no conclusion on the scenario for mass dependent or independent. However, if we fit firstly π^- and K^- , and then including \bar{p} , we can see T_0 (β_T) increases obviously (decreases slightly) with increasing the mass. Thus, we observed the mass dependent or differential kinetic freeze-out.

It should be noted that although Figure 4 also shows the enhancement of T when m_0 increases, this has been observed for many experiments and for the first time was reported by NA44 Collaboration [45] as evidence of the flow. That result is from a fit of p_T to a thermal model for π^- , K^- , and \bar{p} . This means maybe that the

use of the two-component source model is unnecessary to get the enhancement of T when m_0 increases. In fact, although using a single component source model can get the similar conclusion, the two-component source model can describe well the p_T spectra. In addition, including together the hard component, the model can describe better the p_T spectra.

The mass dependence of T (T_0) and β_T is exist because it reflects the mass dependence of $\langle p_T \rangle$. We do not think that the mass dependence of T (T_0) and β_T is a model dependence, though the values of T (T_0) and β_T themselves are model dependent. In our fits, we have used the same p_T range for π^- , K^- , and \bar{p} , while in the blast-wave fit different p_T ranges are used for the three types of particles [2]. The treatment by the latter increases the flexibility in the selection of parameters.

Figure 5(a) shows the dependences of kinetic freeze-out volume V on rest mass m_0 for productions of negative charged particles in central and peripheral Au-Au collisions at $\sqrt{s_{NN}} = 62.4$ GeV as well as in pp collisions at $\sqrt{s} = 62.4$ GeV, while Figure 5(b) gives the dependences of V on m_0 for negative charged particles produced in central and peripheral Pb-Pb collisions at $\sqrt{s_{NN}} = 5.02$ TeV as well as in pp collisions at $\sqrt{s} = 5.02$ TeV. The filled, empty, and half filled symbols represent the central AA , peripheral AA and pp collisions respectively and they represent the results weighted different contribution fractions (volumes) in two components listed in Table 1.

It can be seen from Figure 5 that V in central AA collisions for all the particles are larger than those in peripheral AA collisions, which shows more participant nucleons and larger expansion in central AA collisions as compared to peripheral AA collisions. Meanwhile, V in pp collisions is less than that in peripheral AA collisions of the same $\sqrt{s_{NN}}$ (\sqrt{s}), which is caused by the less participant nucleons (less multiplicity) in pp collisions. It is also observed that V decreases with the increase of m_0 . This leads to a volume dependent or differential freeze-out scenario and indicates different freeze-out surfaces for different particles, depending on their masses that show the early freeze-out of heavier particles as compared to the lighter particles [10, 11].

Figure 6 shows the dependences of T on V for productions of negative charged particles in (a) central and peripheral Au-Au collisions as well as in pp collisions at 62.4 GeV, and in (b) central and peripheral Pb-Pb collisions as well as in pp collisions at 5.02 TeV. The filled,

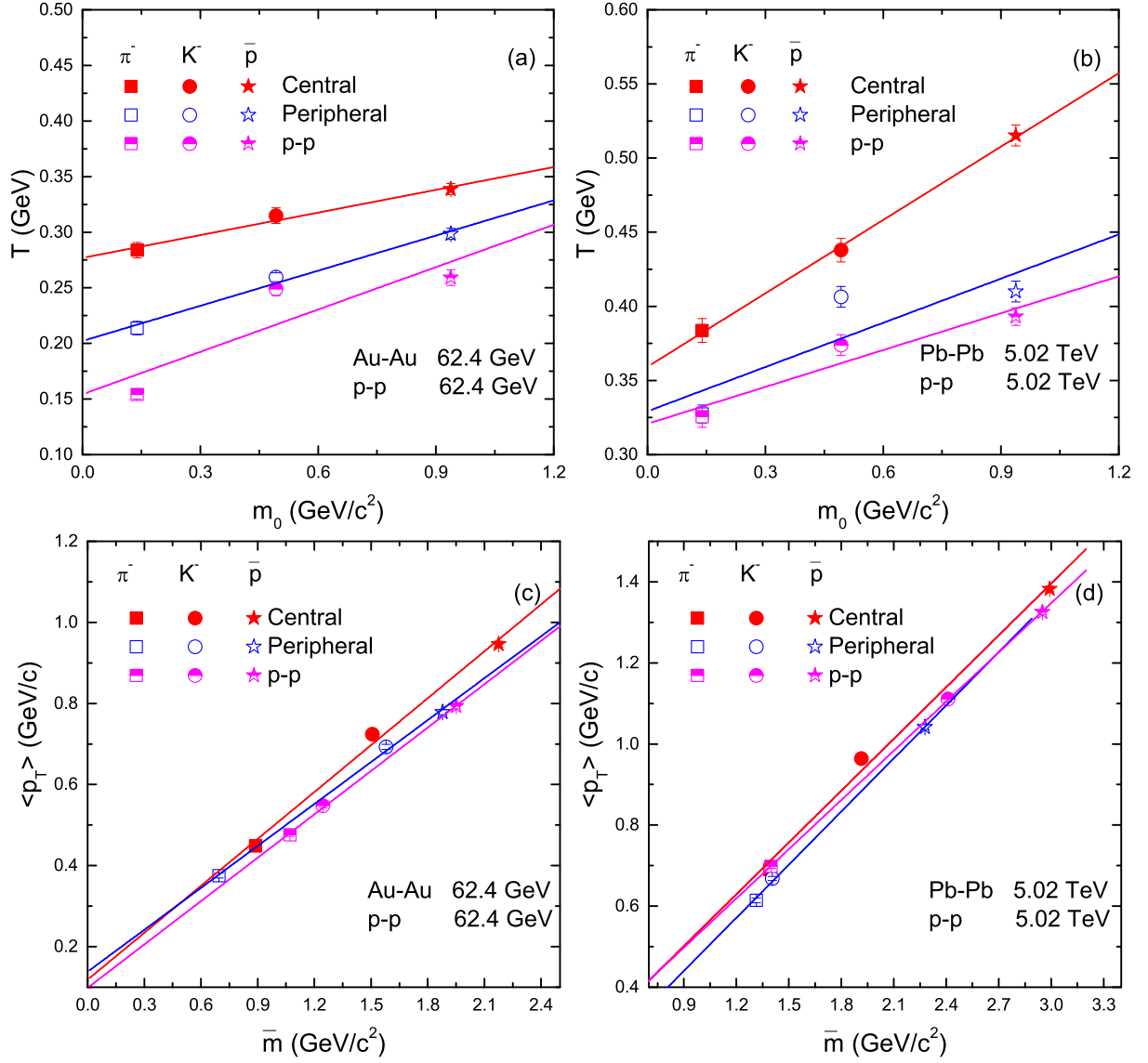


Fig. 4. Dependences of (a)(b) T on m_0 and (c)(d) $\langle p_T \rangle$ on \bar{m} for negative charged particles produced in (a)(c) central and peripheral Au-Au collisions as well as pp collisions at 62.4 GeV, and in (b)(d) central and peripheral Pb-Pb collisions as well as pp collisions at 5.02 TeV. The filled, empty, and half filled symbols represent the parameter values from central and peripheral AA and pp collisions respectively. The lines are linear fits for the parameter values.

empty, and half filled symbols represent central and peripheral AA and pp collisions respectively. One can see that T decreases with the increase of V in central and peripheral AA and pp collisions. This result is natural due to the fact that a large V corresponds to a long kinetic freeze-out time and then a cool system and a low T .

Because of no systematic analysis on the mass dependence of T_0 (β_T) being done in the present work, we shall not study the relation between T_0 (β_T) and V anymore,

though we can predict the trend. As a supplement, our recent work [46] reported the mass dependence (slightly dependence) of T_0 (β_T) by the same method as used in the present work, but using the Tsallis distribution as the “thermometer”. We understand that with increasing m_0 (decreasing V), T_0 increase obviously, and β_T decreases slightly.

From Figures 4–6 one can also see that T , T_0 , β_T , and V obtained from collisions at the LHC are larger than those obtained from collisions at the RHIC. These

Table 2. Values of slopes, intercepts, and χ^2 in the linear relations $T = am_0 + T_0$ and $\langle p_T \rangle = \beta_T \bar{m} + b$, where T , m_0 (\bar{m}) and $\langle p_T \rangle$ are in the units of GeV, GeV/ c^2 and GeV/ c respectively.

Figure	Relation	$\sqrt{s_{NN}}$ (\sqrt{s})	Collisions	a (c^2), β_T (c)	T_0 (GeV), b (GeV/ c)	χ^2
Figure 4(a)	$T - m_0$	62.4 GeV	Central Au-Au	0.0679 ± 0.006	0.2769 ± 0.006	1
			Peripheral Au-Au	0.1054 ± 0.005	0.2022 ± 0.004	1
			pp	0.1270 ± 0.005	0.1543 ± 0.006	40
Figure 4(b)	$T - m_0$	5.02 TeV	Central Pb-Pb	0.1650 ± 0.004	0.3593 ± 0.006	1
			Peripheral Pb-Pb	0.0994 ± 0.005	0.3293 ± 0.005	31
			pp	0.0829 ± 0.005	0.3208 ± 0.006	6
Figure 4(c)	$\langle p_T \rangle - \bar{m}$	62.4 GeV	Central Au-Au	0.3857 ± 0.004	0.1186 ± 0.006	23
			Peripheral Au-Au	0.3449 ± 0.006	0.1381 ± 0.004	5
			pp	0.3567 ± 0.006	0.0983 ± 0.005	1
Figure 4(d)	$\langle p_T \rangle - \bar{m}$	5.02 TeV	Central Pb-Pb	0.4260 ± 0.006	0.1178 ± 0.005	37
			Peripheral Pb-Pb	0.4371 ± 0.005	0.0465 ± 0.004	2
			pp	0.4048 ± 0.006	0.1331 ± 0.005	1

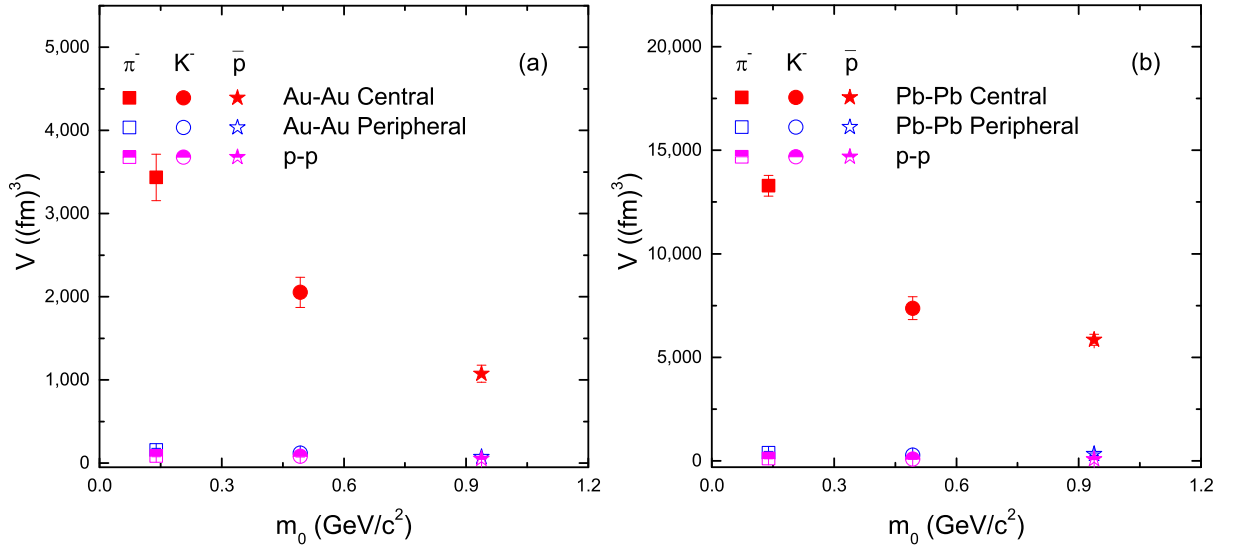


Fig. 5. Dependences of V on m_0 for negative charged particles produced in (a) central and peripheral Au-Au collisions as well as pp collisions at 62.4 GeV, and in (b) central and peripheral Pb-Pb collisions as well as pp collisions at 5.02 TeV. The filled, empty, and half filled symbols represent the parameter values from central and peripheral AA and pp collisions respectively.

results are natural due to more violent collisions happening at higher energy. However, from the RHIC to LHC, the increase of collision energy is obviously large, and the increases of T , T_0 , β_T , and V are relatively small. This reflects the penetrability of projectile in the transparent target. In addition, pions correspond obviously to a larger V than protons in some cases. This is caused by the fact that, pions have larger β_T and then reach larger space than protons due to less m_0 of the former, at similar momenta for pions and protons

at the kinetic freeze-out. This guess is true due to V being a reflection of multiplicity, and experimental results indicate an enhancement of the hadron source as the multiplicity does.

The result that pions correspond to a much larger V than protons means that the protons stop interacting while pions are still interacting. In fact, one may think that pions and protons stop their interacting in different V , where large V corresponds to long interacting time. Because of protons having larger m_0 than pions,

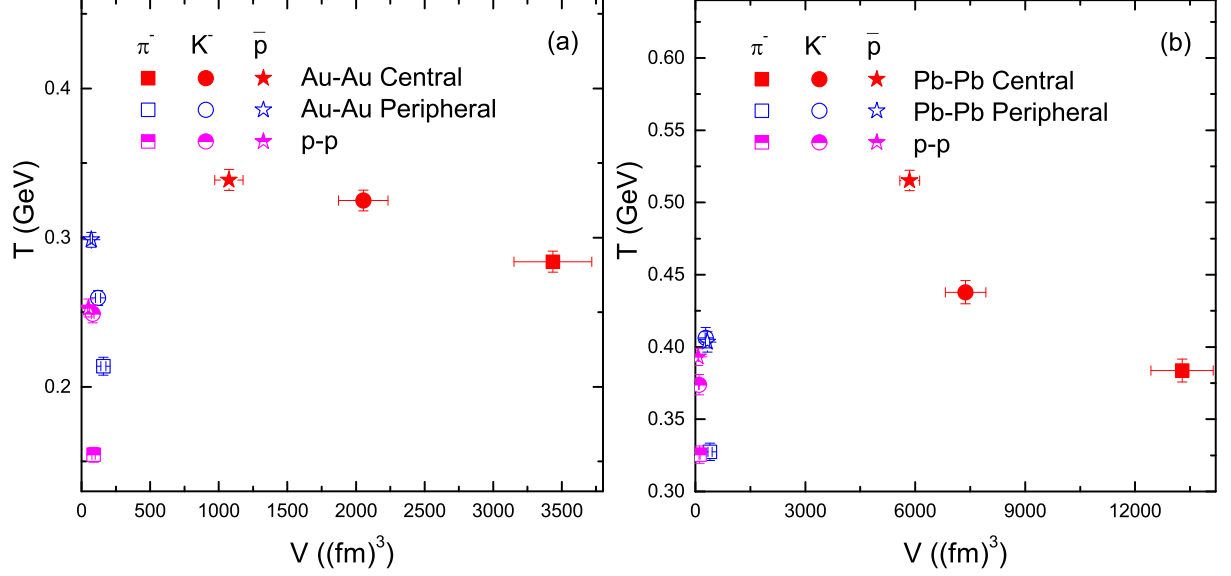


Fig. 6. Same as Figure 5, but showing the dependences of T on V .

Table 3. Values of $\langle T \rangle$ and $\langle V \rangle$ in different types of collisions at the RHIC and LHC. The average values are obtained by different weights due to different contribution fractions (V) of π^- , K^- and \bar{p} .

Figure	$\sqrt{s_{NN}}$ (\sqrt{s})	Collisions	$\langle T \rangle$ (GeV)	$\langle V \rangle$ (fm^3)
Figure 1(a)	62.4 GeV	Central Au-Au	0.303 ± 0.007	2610 ± 218
Figure 1(b)		Peripheral Au-Au	0.247 ± 0.007	130 ± 17
Figure 3(a)		pp	0.214 ± 0.006	77 ± 10
Figure 2(a)	5.02 TeV	Central Pb-Pb	0.478 ± 0.009	10002 ± 658
Figure 2(b)		Peripheral Pb-Pb	0.374 ± 0.008	344 ± 54
Figure 3(b)		pp	0.360 ± 0.006	100 ± 13

protons are leaved behind during the system evolution from the origin of collisions to radial direction, which is the behavior of hydrodynamics [47]. This results in the volume dependent freeze-out scenario which shows the early freeze-out of heavier particles as compared to the lighter particles [10, 11]. Then, pions correspond to larger interacting volume than protons, at the stage of kinetic freeze-out.

To study further the dependences of T and V on centrality and collisions energy, Table 3 contains the values of average T ($\langle T \rangle$) and average V ($\langle V \rangle$) for different types of collisions at the RHIC and LHC. These averages are obtained by different particle weights due to different contribution fractions (V) of π^- , K^- and \bar{p} . One can see clearly that $\langle T \rangle$ and $\langle V \rangle$ at the LHC are larger than those at the RHIC. Generally, T happens between T_{ch} and T_0 . In particular, T_{ch} in central AA

collisions is about 160 MeV, and T_0 in central AA collisions is less than 130 MeV [30, 31, 48, 49]. However, the values of $\langle T \rangle$ in Table 3 are larger because of Eq. (4) being used. In fact, Eq. (4) contains the contributions of both thermal motion and flow effect, which can be regarded as a different “thermometer” from literature [30, 31, 48, 49, 50], which results in different T which is beyond the general range of $[T_{ch}, T_0]$.

Even for T_0 (the intercept in Table 2 for Figs. 4(a) and 4(b)) obtained from $T = am_0 + T_0$, one can see larger values. This is caused by the different “thermometers” being used. If one uses other fit functions [29, 30, 31, 32, 33], the obtained T_0 will be larger or smaller, which depends on the fit function itself. For β_T (the slope in Table 2 for Figs. 4(c) and 4(d)) obtained from $\langle p_T \rangle = \beta_T \overline{m} + b$, one can see different values from other methods (“thermometers”) [20, 21, 22, 26].

Anyhow, the relative sizes of T_0 (β_T) obtained from the present work for different event centralities, system sizes, and collision energies are useful and significative. Generally, $T_0 \leq T_{ch}$. However, because different “thermometers” are used, it is not simple if we compare the two temperatures directly.

Although the absolute values of T (T_0) and β_T obtained in the present work are possibly inconsistent with other results, the relative values are clearly worth considering. Similar situation is true for V . The present work shows that V in central and peripheral Pb-Pb and pp collisions at 5.02 TeV is also larger than that in central and peripheral Au-Au and pp collisions at 62.4 GeV. This shows strong dependence of parameters on collision energy. Furthermore, V in central and peripheral Pb-Pb collisions is larger than that in central and peripheral Au-Au collisions that also shows somehow parameter dependence on size of the system, though this dependence can be neglected due to small difference in the size. The dependence of collision energy and system size is not discussed here in detail because of the unavailability of wide range of analysis but it can be focused in the future work.

3.3 Further discussion

Before summary and conclusions, we would like to point out that the method that the related parameters can be extracted from the p_T spectra of identified particles seems approximately effective in high energy collisions. In fact, at high energy (dozens of GeV and above), the particle dependent chemical potential μ is less than several MeV which affects indeed less the parameters. Eqs. (1)–(4) can be used in the present work. We think that our result on the source volume for pp collisions being larger than that ($\sim 34 \text{ fm}^3$) by the femtoscopy with two-pion Bose-Einstein correlations [51] is caused by different methods.

At intermediate and low energies, the method used here seems possibly unsuitable due to the fact that the particle dependent μ at the kinetic freeze-out is large and unavailable. In general, the particles of different species develop different μ from chemical freeze-out to kinetic freeze-out. This seems to result in more difficult application of Eqs. (1)–(4) at intermediate and low energies. In fact, μ has less influence on the extraction of source volume due to its less influence on the data normalization or multiplicity.

As we know, the source volume is proportional to the

data normalization or multiplicity. Although we can obtain the normalization or multiplicity from a model, the obtained value is almost independent of model. In other words, the normalization or multiplicity reflects the data itself, but not the model itself. Different methods do not affect the source volume obviously due to the normalization or multiplicity being the most main factor, if not the only one. In the case of using considerable μ , neglecting the radial flow and using T , there is no obvious influence on the normalization or multiplicity, then on the source volume.

In addition, although we use the method of linear relation to obtain T_0 and β_T in the present work, we have used the blast-wave model [20, 21, 26, 29] to obtain the two parameters in our previous works [22, 43, 44]. Besides, we could add indirectly the flow velocity in the treatment of standard distribution [52]. Because of different “thermometers” (fit functions) being used in different methods, the “measured” temperatures are different in the value, though the same trend can be observed in the same or similar collisions. The results obtained from different “thermometers” can be checked each other.

In particular, we have obtained the higher temperature, though it is also the kinetic freeze-out temperature and describes the excitation degree of emission source at the stage of kinetic freeze-out. We cannot compare the T_0 obtained in the present work with T_{ch} used in literature directly due to different “thermometers”. We have found that the present work gives the same trend for main parameters when we compare them with our previous works [22, 43, 44] which used the blast-wave model [20, 21, 26, 29]. As it may, the relative size of main parameters in central and peripheral collisions as well as in AA and pp collisions are the same if we use the standard distribution and the blast-wave model.

It should be point out that, although we have studied some parameters at the stage of kinetic freeze-out, the parameters at the stage of chemical freeze-out are lacking in this paper. In fact, the parameters at the stage of chemical freeze-out are more important [53, 54, 55, 56, 57, 58] to map the phase diagram in which μ is necessary essential factor. Both the T_{ch} and μ are the most important parameters at the stage of chemical freeze-out. In the extensive statistics and/or axiomatic/generic non-extensive statistics [53, 54, 55], one may discuss the chemical and/or kinetic freeze-out parameters systematically.

Reference [56] has tried to advocate a new parametrization procedure rather than the standard χ^2 procedure with yields, the authors have constructed the mean value of conserved charges and have utilized their ratios to extract T_{ch} and μ . Reference [57] has evaluated systematic error arising due to the chosen set of particle ratios and constraints. A centrality dependent study for the chemical freeze-out parameters [58] can be obtained. Meanwhile, with the help of the single-freeze-out model in the chemical equilibrium framework [59, 60], Reference [61] has studied the centrality dependence of freeze-out temperature fluctuations in high energy AA collisions.

We are very interested to do a uniform study on the chemical and kinetic freeze-out parameters in future. Meanwhile, the distribution characteristics of various particles produced in high energy collisions are very abundant [62, 63, 64, 65], and the methods of modelling analysis are multiple. We hope to study the spectra of multiplicities, transverse energies, and transverse momenta of various particles produced in different collisions by a uniform method, in which the probability density function contributed by each participant parton is considered carefully.

4 Summary and conclusions

We summarize here our main observations and conclusions

(a) The main parameters extracted from the transverse momentum spectra of identified particles produced in central and peripheral Au-Au collisions at 62.4 GeV and Pb-Pb collisions at 5.02 TeV are studied. Furthermore, the same analysis is done for pp collisions at both RHIC and LHC energies. The two-component standard distribution is used, which includes both the very soft and soft excitation processes. The effective temperature, kinetic freeze-out temperature, transverse flow velocity, and kinetic freeze-out volume are larger in central collisions as compared to peripheral collisions, which shows higher excitation and larger expansion in central collisions.

(b) The effective temperatures in the central and peripheral Au-Au (Pb-Pb) collisions at the RHIC (LHC) are observed to increase with increasing the particle mass, which shows a mass dependent differential kinetic freeze-out scenario at RHIC and LHC energies. The kinetic freeze-out temperature is also expected to in-

crease with increasing the particles mass. The kinetic freeze-out volume decrease with the increase of particle mass that shows different values for different particles and it indicates the volume dependent differential kinetic freeze-out scenario. The transverse flow velocity is expected to decrease slightly with the increase of particle mass.

(c) The effective (kinetic freeze-out) temperatures in peripheral Au-Au and pp collisions at 62.4 GeV as well as in peripheral Pb-Pb and pp collisions at 5.02 TeV are respectively similar and have similar trend, which show similar thermodynamic nature of the parameters in peripheral AA and pp collisions at the same center-of-mass energy (per nucleon pair). The effective (kinetic freeze-out) temperatures in both central and peripheral AA and pp collisions decrease with the increase of the kinetic freeze-out volume. The transverse flow velocity is expected to increase slightly with the increase of the kinetic freeze-out volume in the considered energy range.

(d) The effective (kinetic freeze-out) temperature, transverse flow velocity, and kinetic freeze-out volume in central and peripheral AA and pp collisions at the LHC are larger than those at the RHIC, which shows their dependence on collision energy. Also, central (peripheral) Pb-Pb collisions give slightly larger effective (kinetic freeze-out) temperature, transverse flow velocity, and kinetic freeze-out volume than central (peripheral) Au-Au collisions. This shows somehow parameter dependence on the size of the system, which can be neglected for Pb-Pb and Au-Au collisions due to their small difference in the size.

Acknowledgments

This work was supported by the National Natural Science Foundation of China under Grant Nos. 11575103 and 11947418, the Chinese Government Scholarship (China Scholarship Council), the Scientific and Technological Innovation Programs of Higher Education Institutions in Shanxi (STIP) under Grant No. 201802017, the Shanxi Provincial Natural Science Foundation under Grant No. 201901D111043, and the Fund for Shanxi “1331 Project” Key Subjects Construction.

References

- [1] N. Xu, (for the STAR Collaboration), An overview of STAR experimental results. *Nucl. Phys. A* **931**, 1 (2014). <https://doi.org/10.1016/j.nuclphysa.2014.10.022>
- [2] S. Chatterjee, S. Das, L. Kumar et al., Freeze-out parameters in heavy-ion collisions at AGS, SPS, RHIC, and LHC energies. *Adv. High Energy Phys.* **2015**, 349013 (2015). <https://doi.org/10.1155/2015/349013>
- [3] S. Chatterjee, B. Mohanty, R. Singh, Freezeout hypersurface at energies available at the CERN Large Hadron Collider from particle spectra: Flavor and centrality dependence. *Phys. Rev. C* **92**, 024917 (2015). <https://doi.org/10.1103/PhysRevC.92.024917>
- [4] S. Chatterjee, B. Mohanty, Production of light nuclei in heavyion collisions within a multiple-freezeout scenario. *Phys. Rev. C* **90**, 034908 (2014). <https://doi.org/10.1103/PhysRevC.90.034908>
- [5] S. S. Räsänen, (for the ALICE Collaboration), ALICE overview. *EPJ Web Conf.* **126**, 02026 (2016). https://doi.org/10.1051/epj_conf/201612602026
- [6] X.-F. Luo, N. Xu, Search for the QCD critical point with fluctuations of conserved quantities in relativistic heavy-ion collisions at RHIC: an overview. *Nucl. Sci. Tech.* **28**, 112 (2017). <https://doi.org/10.1007/s41365-017-0257-0>
- [7] H.C. Song, Y. Zhou, K. Gajdošová, Collective flow and hydrodynamics in large and small systems at the LHC. *Nucl. Sci. Tech.* **28**, 99 (2017). <https://doi.org/10.1007/s41365-017-0245-4>
- [8] G. Bertsch, P. J. Siemens, Nuclear fragmentation. *Phys. Lett. B* **126**, 9 (1983). [https://doi.org/10.1016/0370-2693\(83\)90004-7](https://doi.org/10.1016/0370-2693(83)90004-7)
- [9] L.G. Moretto, G.J. Wozniak, Multifragmentation in heavy ion processes. *Ann. Rev. Nucl. Part. Sci.* **43**, 379 (1993). <https://doi.org/10.1146/annurev.ns.43.120193.002115>
- [10] D. Thakur, S. Tripathy, P. Garg et al., Indication of differential kinetic freeze-out at RHIC and LHC energies. *Acta Phys. Pol. B Proc. Supp.* **9**, 329 (2016). <https://www.actaphys.uj.edu.pl/S/9/2/329/pdf>
- [11] D. Thakur, S. Tripathy, P. Garg et al., Indication of a differential freeze-out in proton-proton and heavy-ion collisions at RHIC and LHC energies. *Adv. High Energy Phys.* **2016**, 4149352 (2016). <https://doi.org/10.1155/2016/4149352>
- [12] D.H.E. Gross, Microcanonical thermodynamics and statistical fragmentation of dissipative systems: The topological structure of the N -body phase space. *Phys. Rept.* **279**, 119 (1997). [https://doi.org/10.1016/S0370-1573\(96\)00024-5](https://doi.org/10.1016/S0370-1573(96)00024-5)
- [13] B. Borderie, Dynamics and thermodynamics of the liquid-gas phase transition in hot nuclei studied with the INDRA array. *J. Phys. G* **28**, R217 (2002). <https://doi.org/10.1088/0954-3899/28/8/201>
- [14] M. D'Agostino, F. Gulminelli, P. Chomaz et al., Negative heat capacity in the critical region of nuclear fragmentation: an experimental evidence of the liquid-gas phase transition. *Phys. Lett. B* **473**, 219 (2000). [https://doi.org/10.1016/S0370-2693\(99\)01486-0](https://doi.org/10.1016/S0370-2693(99)01486-0)
- [15] M. D'Agostino, R. Bougault, F. Gulminelli et al., On the reliability of negative heat capacity measurements. *Nucl. Phys. A* **699**, 795 (2002). [https://doi.org/10.1016/S0375-9474\(01\)01287-8](https://doi.org/10.1016/S0375-9474(01)01287-8)
- [16] P. Chomaz, V. Duflot, F. Gulminelli, Caloric curves and energy fluctuations in the microcanonical liquid-gas phase transition. *Phys. Rev. Lett.* **85**, 3587 (2000). <https://doi.org/10.1103/PhysRevLett.85.3587>
- [17] R. Hagedorn, Multiplicities, p_T distributions and the expected hadron \rightarrow quark-gluon phase transition. *Riv. Nuovo Cimento* **6**(10), 1 (1983). <https://doi.org/10.1007/BF02740917>
- [18] J. Cleymans, D. Worku, Relativistic thermodynamics: Transverse momentum distributions in high-energy physics. *Eur. Phys. J. A* **48**, 160 (2012). <https://doi.org/10.1140/epja/i2012-12160-0>
- [19] H. Zheng, L.L. Zhu, Comparing the Tsallis distribution with and without thermodynamical description in $p + p$ collisions. *Adv. High Energy Phys.* **2016**, 9632126 (2016). <https://doi.org/10.1155/2016/9632126>
- [20] Z.B. Tang, Y.C. Xu, L.J. Ruan et al., Spectra and radial flow in relativistic heavy ion collisions with Tsallis statistics in a blast-wave description. *Phys. Rev. C* **79**, 051901(R) (2009). <https://doi.org/10.1103/PhysRevC.79.051901>
- [21] E. Schnedermann, J. Sollfrank, U.W. Heinz, Thermal phenomenology of hadrons from 200A GeV S+S collisions. *Phys. Rev. C* **48**, 2462 (1993). <https://doi.org/10.1103/PhysRevC.48.2462>
- [22] H.-L. Lao, F.-H. Liu, B.-C. Li et al., Kinetic freeze-out temperatures in central and peripheral collisions: which one is larger?. *Nucl. Sci. Tech.* **29**, 82 (2018). <https://doi.org/10.1007/s41365-018-0425-x>
- [23] H.-L. Lao, F.-H. Liu, B.-C. Li et al., Examining the model dependence of the determination of kinetic freeze-out temperature and transverse flow velocity in small collision system. *Nucl. Sci. Tech.* **29**, 164 (2018). <https://doi.org/10.1007/s41365-018-0504-z>

- [24] H.-R. Wei, F.-H. Liu, R.A. Lacey, Kinetic freeze-out temperature and flow velocity extracted from transverse momentum spectra of final-state light flavor particles produced in collisions at RHIC and LHC. *Eur. Phys. J. A* **52**, 102 (2016). <https://doi.org/10.1140/epja/i2016-16102-6>
- [25] H.-R. Wei, F.-H. Liu, R.A. Lacey, Disentangling random thermal motion of particles and collective expansion of source from transverse momentum spectra in high energy collisions. *J. Phys. G* **43**, 125102 (2016). <https://doi.org/10.1088/0954-3899/43/12/125102>
- [26] B.I. Abelev et al., (STAR Collaboration), Systematic measurements of identified particle spectra in pp , $d+Au$, and $Au+Au$ collisions at the STAR detector. *Phys. Rev. C* **79**, 034909 (2009). <https://doi.org/10.1103/PhysRevC.79.034909>
- [27] S. Takeuchi, K. Murase, T. Hirano et al., Effects of hadronic rescattering on multistrange hadrons in high-energy nuclear collisions. *Phys. Rev. C* **92**, 044907 (2015). <https://doi.org/10.1103/PhysRevC.92.044907>
- [28] H. Heiselberg, A.-M. Levy, Elliptic flow and HanburyCBrownC Twiss correlations in noncentral nuclear collisions. *Phys. Rev. C* **59**, 2716 (1999). <https://doi.org/10.1103/PhysRevC.59.2716>
- [29] B.I. Abelev et al., (STAR Collaboration), Identified particle production, azimuthal anisotropy, and interferometry measurements in $Au+Au$ collisions at $\sqrt{s_{NN}} = 9.2$ GeV. *Phys. Rev. C* **81**, 024911 (2010). <https://doi.org/10.1103/PhysRevC.81.024911>
- [30] J. Cleymans, H. Oeschler, K. Redlich et al., Comparison of chemical freeze-out criteria in heavy-ion collisions. *Phys. Rev. C* **73**, 034905 (2006). <https://doi.org/10.1103/PhysRevC.73.034905>
- [31] A. Andronic, P. Braun-Munzinger, J. Stachel, Hadron production in central nucleus-nucleus collisions at chemical freeze-out. *Nucl. Phys. A* **772**, 167 (2006). <https://doi.org/10.1016/j.nuclphysa.2006.03.012>
- [32] S. Uddin, J.S. Ahmad, W. Bashir et al., A unified approach towards describing rapidity and transverse momentum distributions in a thermal freeze-out model. *J. Phys. G* **39**, 015012 (2012). <https://doi.org/10.1088/0954-3899/39/1/015012>
- [33] R.P. Adak, S. Das, S.K. Ghosh et al., Centrality dependence of chemical freeze-out parameters from net-proton and net-charge fluctuations using a hadron resonance gas model. *Phys. Rev. C* **96**, 014902 (2017). <https://doi.org/10.1103/PhysRevC.96.014902>
- [34] R. Odorico, Does a transverse energy trigger actually trigger on large- p_T jets?. *Phys. Lett. B* **118**, 151 (1982). [https://doi.org/10.1016/0370-2693\(82\)90620-7](https://doi.org/10.1016/0370-2693(82)90620-7)
- [35] K. Aamodt et al. (ALICE Collaboration), Transverse momentum spectra of charged particles in proton-proton collisions at $\sqrt{s} = 900$ GeV with ALICE at the LHC. *Phys. Lett. B* **693**, 53 (2010). <https://doi.org/10.1016/j.physletb.2010.08.026>
- [36] T. Mizoguchi, M. Biyajima, N. Suzuki, Analyses of whole transverse momentum distributions in $p\bar{p}$ and pp collisions by using a modified version of Hagedorn's formula. *Int. J. Mod. Phys. A* **32**, 1750057 (2017). <https://doi.org/10.1142/S0217751X17500579>
- [37] H.-L. Lao, Y.-Q. Gao, F.-H. Liu, Light particle and quark chemical potentials from negatively to positively charged particle yield ratios corrected by removing strong and weak decays. *Adv. High Energy Phys.* **2020**, 5064737 (2020). <https://doi.org/10.1155/2020/5064737>
- [38] M. Shao (for the STAR Collaboration), Pion, kaon and (anti-)proton production in $Au+Au$ collisions at $\sqrt{s_{NN}} = 62.4$ GeV. *J. Phys. G* **31**, S85 (2005). <https://doi.org/10.1088/0954-3899/31/4/011>
- [39] Y.C. Morales, N. Hussain, N. Jacazio et al., Production of pions, kaons and protons in pp and $Pb-Pb$ collisions at $\sqrt{s} = 5.02$ TeV. CERN Preprint (ALICE Analysis Note 2016) ALICE-ANA-2016-xxx (July 12, 2017). <http://alice-notes.web.cern.ch/>
- [40] S. Acharya et al., (ALICE Collaboration), Production of charged pions, kaons, and (anti-)protons in $Pb-Pb$ and inelastic pp collisions at $\sqrt{s_{NN}} = 5.02$ TeV. *Phys. Rev. C* **101**, 044907 (2020). <https://doi.org/10.1103/PhysRevC.101.044907>
- [41] A. Adare et al., (PHENIX Collaboration), Identified charged hadron production in $p + p$ collisions at $\sqrt{s} = 200$ and 62.4 GeV. *Phys. Rev. C* **83**, 064903 (2011). <https://doi.org/10.1103/PhysRevC.83.064903>
- [42] P.-P. Yang, M.-Y. Duan, F.-H. Liu et al., Multi-particle production and initial quasitemperature from proton-induced carbon collisions at $p_{Lab} = 31$ GeV/c. *Adv. High Energy Phys.* **2020**, 9542196 (2020). <https://doi.org/10.1155/2020/9542196>
- [43] M. Waqas, F.-H. Liu, S. Fakhreddin et al., Possible scenarios for single, double, or multiple kinetic freeze-out in high-energy collisions. *Indian J. Phys.* **93**, 1329 (2019). <https://doi.org/10.1007/s12648-019-01396-9>
- [44] M. Waqas, F.-H. Liu, Centrality dependence of kinetic freeze-out temperature and transverse flow velocity in high energy nuclear collisions. *Indian J. Phys.*, submitted. arXiv:1806.05863 [hep-ph] (2018). <https://arxiv.org/abs/1806.05863>
- [45] I.G. Bearden et al., (NA44 Collaboration), Collective expansion in high energy heavy ion

- collisions. *Phys. Rev. Lett.* **78**, 2080 (1997). <https://doi.org/10.1103/PhysRevLett.78.2080>
- [46] H.-L. Lao, H.-R. Wei, F.-H. Liu et al., An evidence of mass-dependent differential kinetic freeze-out scenario observed in Pb-Pb collisions at 2.76 TeV. *Eur. Phys. J. A* **52**, 203 (2016). <https://doi.org/10.1140/epja/i2016-16203-2>
- [47] R. Sahoo, Possible formation of QGP-droplets in proton-proton collisions at the CERN Large Hadron Collider. *AAPPS Bulletin* **29**(4), 16 (2019). <https://doi.org/10.22661/AAPPSBL.2019.29.4.16>
- [48] A. Andronic, P. Braun-Munzinger, J. Stachel, Thermal hadron production in relativistic nuclear collisions. *Acta Phys. Pol. B* **40**, 1005 (2009). <https://www.actaphys.uj.edu.pl/R/40/4/1005/pdf>
- [49] A. Andronic, P. Braun-Munzinger, J. Stachel, The horn, the hadron mass spectrum and the QCD phase diagram – the statistical model of hadron production in central nucleus-nucleus collisions. *Nucl. Phys. A* **834**, 237c (2010). <https://doi.org/10.1016/j.nuclphysa.2009.12.048>
- [50] F.G. Gardim, G. Giacalone, M. Luzum et al., Thermodynamics of hot strong-interaction matter from ultrarelativistic nuclear collisions. *Nature Phys.* **16**, 615 (2020). <https://doi.org/10.1038/s41567-020-0846-4>
- [51] K. Aamodt et al., (ALICE Collaboration), Femtoscopy of pp collisions at $\sqrt{s} = 0.9$ and 7 TeV at the LHC with two-pion Bose-Einstein correlations. *Phys. Rev. D* **84**, 112004 (2011). <https://doi.org/10.1103/PhysRevD.84.112004>
- [52] F.-H. Liu, H.-L. Lao, Blast-wave revision of the multisource thermal model in nucleus-nucleus collisions. *Indian J. Phys.* **90**, 1077 (2016). <https://doi.org/10.1007/s12648-016-0846-5>
- [53] A.N. Tawflk, H. Yassin, E.R. Abo Elyazeed, Extensive/nonextensive statistics for p_T distributions of various charged particles produced in p+p and A+A collisions in a wide range of energies. *arXiv:1905.12756 [hep-ph]* (2019). <https://arxiv.org/abs/1905.12756>
- [54] A.N. Tawflk, Axiomatic nonextensive statistics at NICA energies. *Eur. Phys. J. A* **52**, 253 (2016). <https://doi.org/10.1140/epja/i2016-16253-4>
- [55] A.N. Tawflk, H. Yassin, E.R. Abo Elyazeed, Chemical freezeout parameters within generic nonextensive statistics. *Indian J. Phys.* **92**, 1325 (2018). <https://doi.org/10.1007/s12648-018-1216-2>
- [56] S. Bhattacharyya, D. Biswas, S.K. Ghosh et al., Novel scheme for parametrizing the chemical freeze-out surface in heavy ion collision experiments. *Phys. Rev. D* **100**, 054037 (2019). <https://doi.org/10.1103/PhysRevD.100.054037>
- [57] S. Bhattacharyya, D. Biswas, S.K. Ghosh, et al., Systematics of chemical freeze-out parameters in heavy-ion collision experiments. *Phys. Rev. D* **101**, 054002 (2020). <https://doi.org/10.1103/PhysRevD.101.054002>
- [58] D. Biswas, Centrality dependence of chemical freeze-out parameters and strangeness equilibration in RHIC and LHC. *arXiv:2003.10425 [hep-ph]* (2020). <https://arxiv.org/abs/2003.10425>
- [59] D. Prorok, Single freeze-out, statistics and pion, kaon and proton production in central Pb-Pb collisions at $\sqrt{s_{NN}} = 2.76$ TeV. *J. Phys. G* **43**, 055101 (2016). <https://doi.org/10.1088/0954-3899/43/5/055101>
- [60] D. Prorok, Thermal freeze-out versus chemical freeze-out reexamined. *Acta Phys. Pol. B* **40**, 2825 (2009). <https://www.actaphys.uj.edu.pl/R/40/10/2825/pdf>
- [61] D. Prorok, Centrality dependence of freeze-out temperature fluctuations in Pb-Pb collisions at the LHC. *Eur. Phys. J. A* **55**, 37 (2019). <https://doi.org/10.1140/epja/i2019-12709-3>
- [62] L. Zhou, D.-Q. Fang, Effect of source size and emission time on the p-p momentum correlation function in the two-proton emission process. *Nucl. Sci. Tech.* **31**, 52 (2020). <https://doi.org/10.1007/s41365-020-00759-w>
- [63] H. Wang, J.-H. Chen, Y.-G. Ma et al., Charm hadron azimuthal angular correlations in Au+Au collisions at $\sqrt{s_{NN}} = 200$ GeV from parton scatterings. *Nucl. Sci. Tech.* **30**, 185 (2019). <https://doi.org/10.1007/s41365-019-0706-z>
- [64] L.-H. Song, L.-W. Yan, Y. Liu, Constraining the colored $c\bar{c}$ energy loss from J/ψ production in p-A collisions. *Nucl. Sci. Tech.* **29**, 159 (2018). <https://doi.org/10.1007/s41365-018-0502-1>
- [65] S.-H. Zhang, L. Zhou, Y.-F. Zhang et al., Multiplicity dependence of charged particle, ϕ meson, and multi-strange particle productions in p+p collisions at $\sqrt{s} = 200$ GeV from PYTHIA simulation. *Nucl. Sci. Tech.* **29**, 136 (2018). <https://doi.org/10.1007/s41365-018-0469-y>